Article

Not peer-reviewed version

A New Computer Aided Diagnosis for Breast Cancer Detection of Thermograms using Metaheuristic algorithms and Explainable AI

Dihmani Hanane *, Bousselham Abdelmajid *, Bouattane Omar *

Posted Date: 31 August 2024

doi: 10.20944/preprints202408.2279.v1

Keywords: breast cancer detection; thermography; XAI; HPSO; HSMO; Feature extraction; feature attribution; multi-objective optimization; continuous; binary; feature selection; hyperparameter tuning

 doi:10.20944/preprints202408.2279.v1

Article

A New Computer Aided Diagnosis for Breast Cancer Detection of Thermograms Using Metaheuristic algorithms and Explainable AI

Hanane Dihmani [1,*], Abdelmajid Bousselham [2] and Omar Bouattane [1]

[1] Electrical Engineering and Intelligent Systems, ENSET, University Hassan II, Mohammedia, Morocco
[2] Computer science, Artificial Intelligence and Cyber Security, ENSET, University Hassan II, Mohammedia, Morocco
* Correspondence: han.dihmani@gmail.com; Tel.: 00212662482883

Abstract: Advances in early detection of Breast cancer and treatment improvements have significantly increased survival rates. Traditional screening methods, including mammography, MRI, ultrasound, and biopsies, while effective, often come with high costs and risks. Recently, thermal imaging has gained attention due to its minimal risks compared to mammography, although it is not widely adopted as a primary detection tool since it depends on identifying skin temperature changes and lesions. The advent of machine learning (ML) and deep learning (DL) has enhanced the effectiveness of breast cancer detection and diagnosis using this technology. In this study a novel methodology for developing an interpretable computer-aided diagnosis (CAD) system for breast cancer detection, leveraging explainable Artificial Intelligence (XAI) throughout its various phases. To achieve these goals, we proposed a new multi-objective optimization approach named Hybrid Particle Swarm Optimization algorithm (HPSO) and Hybrid spider Monkey Optimization algorithm (HSMO). These algorithms simultaneously combine the continuous and binary representations of PSO and SMO to effectively manage trade-offs between Accuracy, feature selection and hyperparameter tuning. We evaluate several CAD models and investigate the impact of handcrafted methods such as Local Binary Patterns (LBP), Histogram of Oriented Gradients (HOG), Gabor filters, and edge detection. We further shedding light on the effect of feature selection and optimization on feature attribution and model decision-making processes using the SHapley Additive exPlanations (SHAP) framework, with a particular emphasis on cancer classification using the DMR-IR dataset. The results of our experiments demonstrate in all trials that the performance of the model is improved. Also with HSMO our models achieved a high accuracy accuracy of 98.27% and F1- score of 98.15% while selecting only 25.78% of the HOG-features. This approach not only boosts the performance of CAD models but also ensures comprehensive interpretability. This method emerges as a promising and transparent tool for early breast cancer diagnosis.

Keywords: breast cancer detection; thermography; XAI; HPSO; HSMO; Feature extraction; feature attribution; multi-objective optimization; continuous; binary; feature selection; hyperparameter tuning

1. Introduction

Breast cancer is a profoundly distressing disease. Screening programs for early breast disease detection significantly contribute to the reduction of the mortality rate among women. These programs save lives by detecting conditions at their initial stages when treatment is more effective and less costly. Medical imaging modalities are employed for breast cancer diagnosis, as well as the differentiation of malignant from benign breast tumors, including, Mammography, Magnetic Resonance Imaging (MRI), Ultrasound, Computed Tomography (CT), Positron Emission Tomography PET, and thermography. Mammography, while widely used, presents specific limitations. These include challenges in visualizing smaller tumors [1], inadvisability for use in younger women and those with dense breast tissues [**Error! Reference source not found.**], considerable cost and time requirements [3], and physical discomfort due to breast compression. Moreover, concerns about the potential carcinogenic effects of cumulative ionizing radiation

 doi:10.20944/preprints202408.2279.v1

exposure have been raised [**Error! Reference source not found.**]. The high incidence of false-positive results further contributes to patient anxiety and unnecessary procedures [**Error! Reference source not found.**]. In this context, Infrared Thermography has emerged as a promising and robust screening tool for early cancer detection [6–**Error! Reference source not found.**]. Thermography offers distinct advantages, being painless, non-invasive, non-contact, and cost-effective [**Error! Reference source not found.**]. Notably, it is particularly well-suited for screening younger women, patients with dense breast tissue, and pregnant or nursing women, as it does not involve ionizing radiation exposure [**Error! Reference source not found.**].

In health systems, breast cancer diagnostics have benefited from Computer-Aided Diagnosis (CAD) systems, streamlining the analysis process and minimizing errors. These systems typically consist of several steps, from image preprocessing to classification, where feature extraction and selection play vital roles. Extracting pertinent features is essential for capturing subtle patterns indicative of early-stage breast cancer, whether through meticulously crafted methods or advanced deep learning approaches [11]. However, the current narrative predominantly emphasizes the accuracy and automation aspects of these systems, often achieved by training models on extensive datasets to recognize patterns in medical data. Yet, amid these advancements, there exists a notable gap in the discourse – the lack of attention to model interpretability [12]. In this paper, we proposed an interpretable computer-aided diagnosis (CAD), while delving into the relationship between pattern recognition and machine learning. Understanding this connection is paramount in addressing the complexity of medical data. Pattern recognition, within its broader domain, is fundamentally concerned with identifying regularities or inherent patterns within datasets, this field embraces a wide array of techniques and methods designed to identify patterns across various data types, spanning images, signals, and sequences. The attainment of pattern recognition can be realized through two primary approaches: manual and automated. Manual pattern recognition often relies on human expertise and heuristic approaches [13], depending on the nuanced judgment of experts to identify patterns, while automated pattern recognition employs computational methods to autonomously detect and outline patterns embedded within the data [14]. Machine learning, a subset of artificial intelligence, is exclusively dedicated to developing algorithms and statistical models that empower computers to learn from data and subsequently make predictions or decisions, encompassing a vast spectrum of techniques, including supervised learning, unsupervised learning, reinforcement learning, and hybrid methodologies.

On the other hand, Healthcare professionals need to understand how AI systems arrive at their recommendations or decisions, especially when these decisions can have significant real-world impacts. In the context of synergy between pattern recognition and machine learning, Explainable Artificial Intelligence AI (XAI) can be used to understand the rules that are generated, giving insight into the expertise of the medical domain. The evolution and role of XAI in the medical decision-making process have significantly shaped the healthcare industry, offering transparency, trust, and enhanced clinical support (Figure 1) [15,16].

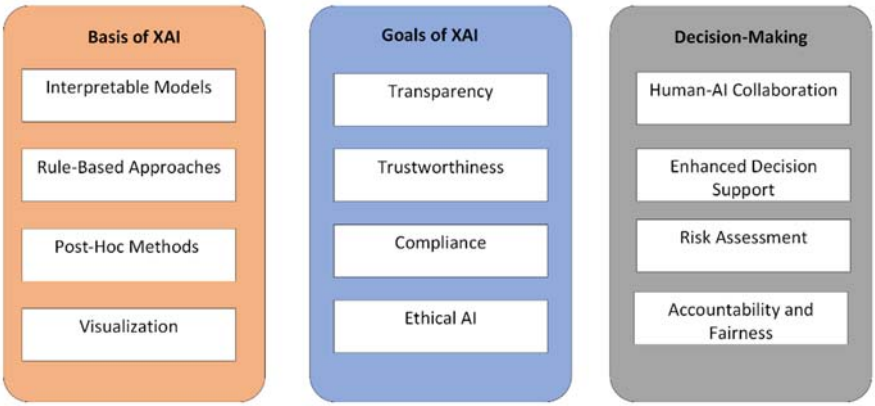

Figure 1. The Evolution and Role of XAI in Decision-Making by stakeholders.

 doi:10.20944/preprints202408.2279.v1

The insights gained by leveraging the integration of machine learning, pattern recognition, and XAI hold significant potential in the domain of medical image analysis for breast cancer detection [17]; each of these fields consists of several processes. One approach that enhances this integration is the use of metaheuristics, which employ techniques inspired by nature to perform abstract optimization [18]. Although a limited number of studies have explored breast cancer thermogram diagnosis using optimization algorithms, the review article [19] presents an overview of advancements in this field. However, many papers often fall short in providing explanations for their outcomes [20].

The authors of this paper are also aware of the ongoing debate surrounding metaheuristic-based optimization [21,22]. In order to address some of those concerns while employing these algorithms, our work stands as a significant contribution to this research area :

1) Our primary goals encompass the comprehensive solution to the challenges of achieving dynamic optimization problems. The development of Hybrid PSO (HPSO) and Hybrid SMO (HSMO) methodologies for tackling continuous variable optimization and discrete problems. The proposed approaches allow the optimization algorithm to ensure effective solutions in a varied search space.
2) Harnessing the power of multi-objective optimization techniques [23], the proposed optimizers aim to provide a deeper understanding of model behavior across varying problem formulations. We used The multi-objective ML approaches to strive to optimize multiple aspects of model performance simultaneously. These include hyperparameter optimization, prediction performance, sparseness, and interpretability.
3) Through our research, an automated aspects on finding textures and features through machine learning based optimization functions that best represent breast cancer classification patterns, by producing handcrafted features from breast thermograms images using different methods, such as LBP, HOG, Gabor and canny edge and SVM for classification are employed.
4) Using visual explanation techniques that generate interpretable graphical representations enables healthcare practitioners to intuitively grasp the rationale behind each classification, making complex patterns associated with breast thermograms more comprehensible.
5) Our HSMO and HPSO optimizer incorporate SHapley Additive **exPlanations** (SHAP) framework into the evaluation process; the method ensures that the importance of different features is considered. This adds another layer of complexity and variation to the solutions being explored.
6) The other goal of this paper is to evaluate the convergence behaviors of distinct metaheuristic algorithms (HPSO, HSMO, Binary Particle Swarm Optimization algorithm (BPSO), and Binary spider Monkey Optimization algorithm (BSMO). to identify similarities and differences in their solutions and secondly, to ensure consistent results upon repeated runs.

The organization of the paper is as follows: Section 2 presents related work. The detailed methodology in Section 3. Section 4 will outline the experimental setup. Section 5 will present the results and related discussions. Finally, Section 6 includes the research conclusion.

2. Related work

2.2. XAI for Medical Image

machine learning models and deep neural networks are often characterized as "black box" models due to their high complexity, resulting in a lack of readily available explanations for their predictions. While these models excel in accuracy, understanding the rationale behind a specific prediction can be a formidable challenge. The inherent non-human-interpretable nature of AI models

 doi:10.20944/preprints202408.2279.v1

has led to limited work aimed at developing models that can effectively elucidate their decision-making processes and actions, as exemplified by the contributions of Kallianos et al [24–28]. There is a growing need for XAI in domains like healthcare, where simply relying on AI for pattern recognition is insufficient. The ability to provide explanations for the decisions made by these models becomes paramount in ensuring that experts within these domains can derive meaningful insights from AI outputs. This ensures transparency and trustworthiness in AI-assisted medical diagnoses, which is essential for gaining acceptance and facilitating collaboration between AI systems and medical professionals [29,30]. Several tools have been developed to enhance the interpretability and explainability of black-box machine learning (ML) models, particularly through visual explanations. Brunese et al. [31] offer explanations for deep learning model predictions for Coronavirus disease (COVID-19) detection, employing Class Activation Maps (CAM). Koyyada and Singh [32] extend this approach by using Gradient CAM (GradCAM). Barata et al. [33] introduce heatmaps that emphasize regions of an image that exerted the most influence on the model's decision. Nigar et al. [34] leverage LIME to interpret deep learning models, providing local insights around specific predictions, as demonstrated in dermatological images.

2.3. XAI- for Breast Thermography

Many papers, such as [35–37], concentrate on the accuracy and automation aspects of using AI for breast cancer classification using thermal imaging. For example, Abdel-Nasser et al. [35] introduced a novel learning technique representation called LTR. By utilizing HOG with 4*4 blocks size and 288 feature vectors, their method achieved an accuracy of 95.80% using an Multi-Layer Perceptron (MLP) classifier. Nevertheless, there are relatively few papers focusing on methods used to aid and assist healthcare professionals or lay individuals in understanding the predictions of machine learning models in breast thermogram images. In a recent study [38,39] authors proposed an approach based on Bayesian Networks BNs with CNNs. The authors emphasize the utilization of BN, which is renowned for its probabilistic and graphical data representation to enhance the interpretability of model predictions. These models extract relevant features from thermography images, which Bayesian Networks can then interpret to make informed and explainable diagnostic decisions. In the study by Nicandro et al. [40], the goal was to evaluate the diagnostic capability of thermographic variables for distinguishing patients suspected of having breast cancer from healthy individuals. The paper employs Bayesian networks for analysis, chosen for their ability to reveal interactions between attributes and classes and interactions among attributes themselves. This unique capability allows for a visual identification of which attributes influence the outcome and how they are interconnected. The results indicate that, while other models like Multi-Layer Perceptrons (MLP) and decision trees demonstrate comparable performance, they lack explanation power. The paper suggests that deep CNN with transfer learning achieves sensitivity levels similar to those of human experts, even in datasets with a low prevalence of breast cancer. The paper by Dey et al. [41] suggests that hybrid of deep CNN and edge detectors can achieve sensitivity levels coparable to those of human experts, even in datasets with a low prevalence of breast cancer. Additionally, they utilized Class Activation Mapping (CAM) into the model. While the paper doesn't explicitly mention the integration of external interpretability beyond CAM, CAM itself serves as a form of explainability by highlighting the regions of interest in the thermograms that contribute to the network's decision-making process.

Considering the advancements of AI for breast cancer detection using thermography, there remains a crucial avenue for improvement, where the scope is placed on optimization-based metaheuristics, a research topic that has garnered significant public attention [42,43]. Furthermore, the demand for elucidating the distinctive contributions of specific models to predictions is more critical than ever. This paper undertakes the challenge of addressing these pivotal aspects and aims to open new research directions by providing an interpretable CAD system capable of handling complex, evolving problems, human interpretability, and feature attribution.

3. Methodology

 doi:10.20944/preprints202408.2279.v1

A multi-step methodology is involved in the proposed CAD architecture. While using LBP as a feature extractor, the complete pipeline is indicated in Figure 2 as follows. The preprocessing of breast thermograms is followed by feature extraction using various texture analysis methods. Next, the extracted features and their histograms are visualized to understand the initial feature vector distribution. Subsequently, the proposed optimization algorithm HPSO and HSMO is employed to identify the most relevant features contributing significantly to the classification task.

Furthermore, recognizing the importance of optimizing model parameters to enhance classification performance, we employ an objective function to ensure optimal performance.

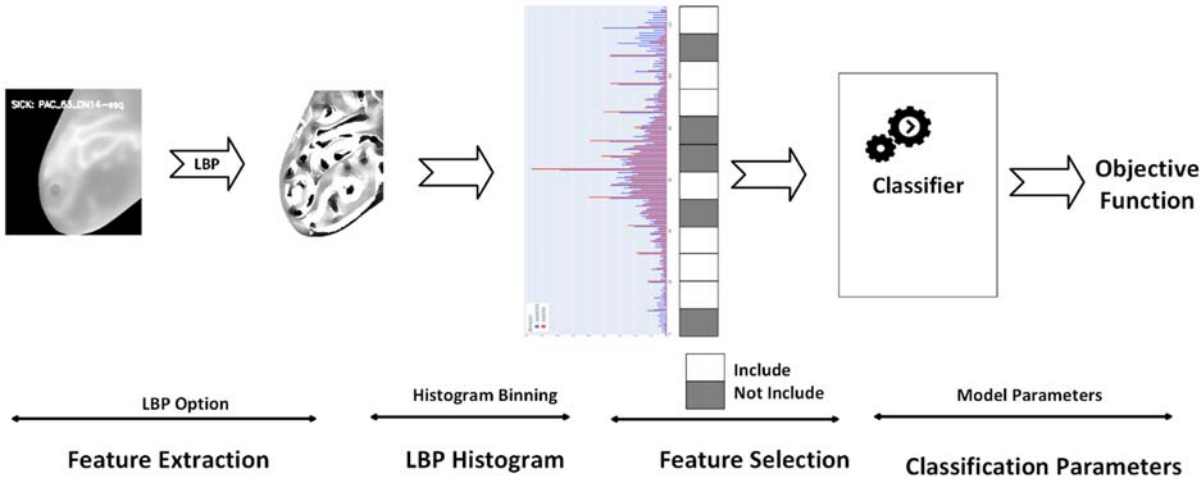

Figure 2. Pipeline Representation

3.1. Dataset Description

This research used images sourced from the Database for Mastology Research with Infrared Image (DMR-IR) [44]. This database contains both Static Infrared Thermography (SIT) and Dynamic Infrared Thermography (DIT) images, with our focus on DIT images. The imaging protocol involves patients standing with their hands on their heads for five minutes. During this period, an electric fan cools the breast and armpit regions in a controlled temperature environment ranging from 20°C to 22°C. Following the cooling phase, a FLIR thermal camera (model SC620) captures 20 DIT images, each with dimensions of 640 × 480 pixels.

This dataset is a comprehensive collection of individual cases designed for breast cancer detection, with each case linked to a unique ID. It offers diversity in terms of age and demographics, encompassing a broad spectrum of breast cancer risk factors. Each case comprises multiple images. The dataset is segregated into two folders "old" cases (Desenvolvimento da Metodologia) and "new" cases (12 Novos Casos de Testes) as shown in Table 1. Notably, each ID in the dataset is labeled as either "healthy" or "sick." Healthy IDs feature images from both the right and left sides of the chest, whereas sick IDs exclusively contain images of the affected side due to differences in temperature gradients between healthy and sick breasts. The conventional approach treats the data as a collection of images split into train/test/validation sets based on predefined ratios [45]. However, this approach introduces a level of data leakage into trained models since each patient ID can have images in multiple sets, potentially causing overlap between the test and training sets. To mitigate this data leakage issue, we propose creating splits based on patient IDs, where each ID's images are associated with one of the possible data splits. The division into test and train sets is initially performed based on IDs and subsequently on their associated images. To achieve this with our proposed approach, we initially gather the IDs and subsequently divide the ID pool into train/test sets, as illustrated in Figure 3. The dataset was split using a 70-30 train-test split ratio. This resulted in 1060 samples allocated for training and 462 samples allocated for testing.

 doi:10.20944/preprints202408.2279.v1

Table 1. Details about dataset classes.

1522 thermogram images (56 subject :37 sick IDs- 19 healthy IDs)					
Desenvolvimento da Metodologia			12 Novos Casos de Testes		
Total	DOENTES (Sick)	SAUDAVEIS (Healthy)	Total	DOENTES (Sick)	SAUDAVEI (Healthy)
1282	640	642	240	120	120

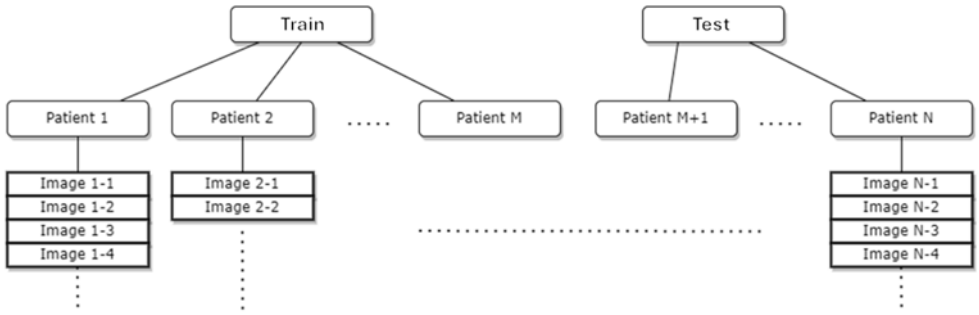

Figure 3. Process of Gathering IDs and Division into Train-Test Sets in DMR-IR database.

3.2. Data Pre-Processing

The pre-processing steps involved several stages to prepare the images for analysis and interpretability. Initially, the heat gradient files were converted into an image format to ensure consistency and compatibility with standard image processing techniques. Next, experts manually segmented the full thermogram images into the chest region, a step included with the dataset. Subsequently, previously segmented grayscale images were cropped to eliminate extraneous regions along each axis. Before feature extraction, the grayscale version of the input image was resized to a standardized dimension of 240×240 pixels to ensure uniformity. Post-feature extraction, an optional normalization, and a rounding step are included, where the features are scaled based on a precomputed scaler from a training dataset. Finally, the selected features were fed into downstream machine learning models for classification.

3.3. Feature Extraction

The feature extraction process is a crucial step in our methodology, enabling the transformation of raw image data into a structured format suitable for machine learning models. We utilize a range of algorithms, namely Histogram of Oriented Gradients (HOG) [46], Local Binary Pattern (LBP) [47], Gabor Filters [48], and Canny edge detection [49]. This diversified strategy aims to capture a comprehensive set of features, taking advantage of each algorithm's unique characteristics [35]. Local Binary Pattern (LBP) encodes the local structure of an image by comparing the intensity of each pixel with its neighboring pixels, providing a robust representation of texture patterns. Gabor Filters analyzes an image's spatial features by capturing the occurrences of pixel patterns with particular intensity values at specific orientations and scales, providing valuable information about the image's texture and structure. Histogram of Oriented Gradients (HOG) divides an image into small regions, computes the gradient and orientation information for each pixel, and then creates a histogram of gradient orientations, capturing the underlying structure of objects. Canny Edge Detection employs a multi-stage algorithm involving gradient computation, non-maximum suppression, and edge tracking with hysteresis to accurately identify and trace edges in an image.

 doi:10.20944/preprints202408.2279.v1

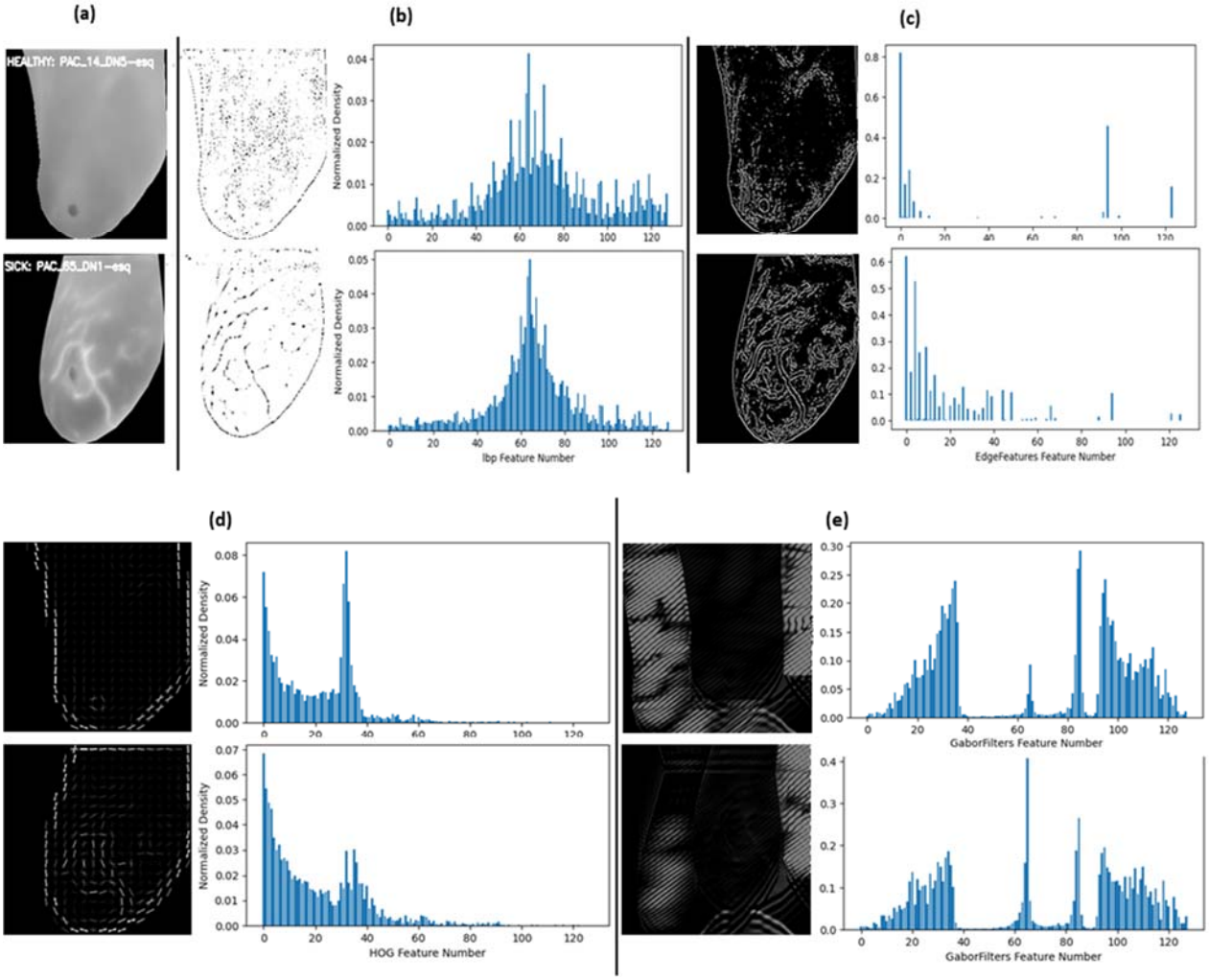

Figure 4. Sample Feature Extract Image and their distributions (a) original cropped image: Top Left healthy sample and Bottom Left sick sample ; (b) LBP; (c) Canny Edges; (d) HOG and (e) Gabor Filter.

It's important to note that the parameters associated with each algorithm are not fixed but are subject to optimization. This flexible approach recognizes the complexity of the dataset, allowing for the fine-tuning of parameters to enhance the performance of the feature extraction process.

Depending on the extractor, the feature vectors are subsequently extracted by dividing all values into N histogram bins, translating each image in the dataset to a feature vector of N length, a feature length of 128 is constructed where each feature is a bin of values representing the frequency or count of a specific pattern in the image. Figure 4 offers sample extractions from each method and their captured data distribution, visually depicting their differences.

The most notable aspect in these samples is that each extractor converted the images into unique sets of feature distributions as well, where the distinctive patterns of classification became varied. This variety was intentional to determine whether the features would align visually when different extractors undergo optimization through metaheuristic algorithms.

3.4. The Proposed Metaheuristic- Based Feature and Hyperparameter Optimization

The metaheuristic algorithms used in our study consist of Spider-Monkey optimization [50] and Particle Swarm [51]. Spider-monkey Optimization (SMO) is a nature-inspired algorithm that draws inspiration from the cooperative foraging behavior of spider monkeys. SMO leverages the concepts of exploration and exploitation to search for optimal solutions in a solution space. The algorithm involves the establishment of a population of potential solutions, and through successive iterations, it refines and evolves these solutions based on the fitness of each candidate. In its binary version, a

 doi:10.20944/preprints202408.2279.v1

boolean operator is used to accomplish this task of transferring continuous solutions in each dimension, which forces the monkey to discretize their movement, representing the presence or absence of a certain feature or decision. The Binary SMO (BSMO) was proposed by Singh et al. [52].

Particle Swarm Optimization (PSO) is a population-based optimization algorithm that simulates the social behavior of birds or fish. Individuals in the population, referred to as particles, traverse the search space, adjusting their positions based on personal experience and the best positions found by their peers. PSO is particularly effective for continuous optimization problems, where variables can take any real value. This algorithm was adapted to work in the binary search space using Binary (BPSO) [53]. The algorithm is known for its simplicity and ability to explore the solution space efficiently.

To find a diverse set of optimal solutions for multi-objective problems, our research employs hybrid versions of these algorithms, integrating both their continuous and binary variables within each algorithm. This hybrid approach allows for a more flexible and adaptable optimization process, addressing the problem of feature selection as well as extractor parameter optimization that involves a mix of discrete and continuous decision variables. Incorporating both variable types enhances the algorithms' capability to handle a broader range of optimization challenges, making them more robust and effective in diverse problem domains.

The HPSO and HSMO codes are depicted in Algorithm 1 and Algorithm 2, respectively.

The values of parameters for the considered algorithms are as follows:

- HPSO and BPSO parameters setting: Inertia Weight (w)=0.5, c1 = 2.0, c2 = 2.0, Population = 10.
- HSMO and BSMO parameters setting: – Population = 10, maximum groups (MG) =2, Global Leader Limit = 20, Local Leader Limit = 20,

In the proposed HSMO algorithm, change_threshold value is modified to dynamically updated at each iteration, the change threshold increment is set to 0.13 and the change threshold initialized to 0.1 and incrementing dynamically using this Equation. The value of change_thresh is typically a value between 0 and 1.

$$change\_thresh \; += \frac{change\_thresh\_increment}{current\ iteration}$$

Algorithm 1 : HPSO

1. Initialize:
   - Initialize the particle positions and velocities.
   - Set parameters like inertia weight (w), cognitive parameter (c1), social parameter (c2), and number of particles (n_particles).
   - Randomly generate initial positions and velocities for particles.
   - Create a DataFrame to store particle information:ID of particle, objective function value, global best position (g_best) and parameters (analogic and continous).
   - Calculate initial objective function values for particles.
   - Set the best positions for each particle and global best position.
2. Iterative Optimization:
   - For a specified number of iterations or until a iteration is met:
     a. Update Velocities:
        - Calculate new velocities for each particle using the formula:

          v(t+1) = w * v(t) + c1 * r1 * (p_best - p(t)) + c2 * r2 * (g_best - p(t))

        - r1 and r2 are random values, p_best is the best position of the particle, and g_best is the global best position.

     b. Update Positions:

 doi:10.20944/preprints202408.2279.v1

- Update the positions of particles using the new velocities.
- For continuous parameters, add the velocity to the position.
- For binary parameters, use a sigmoid function to determine whether to flip the bit based on the velocity.

c. Evaluate Objective Function:

- Calculate the objective function values for the updated positions of the particles.
- Update the DataFrame with the new positions and objective function values.
- Update the best positions for each particle if the new position is better.

d. Update Global Best:

- Determine if any particle's current position is better than the global best position.
- Update the global best position if necessary.

3. Final Output:

- Return the best solution found and its corresponding objective function value.

Algorithm : HSMO

1. Initialize:

- Set parameters like population, parameters (analogic and continous), groups, max_groups, change_threshold, acc_err_delta_threshold, global_lim_thresh, local_lim_thresh, target_value, debug_mode, change_thresh_increment
- Initialize spider monkeys' positions and IDs
- Initialize DataFrame to store positions, fitness, probabilities, etc.
- Calculate initial objective function values and fitness values
- Assign initial probabilities
- Create initial groups
- Identify local leaders and global leader

2. Iterative Optimization:

- For each iteration:

a. Local Leader Phase:

- Randomly select spider monkeys based on change_threshold
- Randomly select group members for value update
- Update positions using local leader and selected group members
- Update fitness values
- Swap positions if fitness improves

b. Global Leader Phase:

- Identify the global leader
- For each group, update positions using global leader and selected group members
- Update fitness values
- Swap positions if fitness improves

c. Local Decision Phase:

- Check if local leader performance improves
- Increment limit count if no improvement
- Reset group if limit count exceeds threshold

d. Global Decision Phase:

 doi:10.20944/preprints202408.2279.v1

- Check if global leader performance improves
- Increment global limit count if no improvement
- Increase number of groups or reset groups if limit count exceeds threshold

e. Update change_threshold

3. Final Output:

- Return the best solution found and its corresponding objective function value

3.5. XAI Models through Metaheuristic Optimization

The XAI model under consideration hinges on the interpretation of features that have undergone a metaheuristic-based optimization process. This optimization ensures that the selected features are not only relevant but also contribute significantly to the model's overall performance. Feature interpretation within our framework is a two-pronged approach aimed at enhancing both robustness and interpretability. First, we utilize Shapley additive explanations (SHAP) to quantify the importance of individual features. This provides a metric for assessing the robustness of the selected features in influencing model outcomes. Second, we implement a visual interpretation strategy by mapping the selected features back onto the original images. This visual mapping facilitates a more intuitive understanding of the role played by specific features in the model's decision-making process. By juxtaposing selected features against their corresponding images, this method provides a tangible link between abstract mathematical representations and real-world visual elements. The combination of these two approaches – quantitative assessment through SHAP and qualitative understanding through visual mapping – not only fortifies the robustness of the XAI model but also introduces a layer of interpretability. Observing and comprehending the features that underpin model decisions is paramount for building trust and facilitating informed decision-making in applications, especially ones related to diagnostic systems such as breast cancer detection for which this study is undertaken.

The Figures below illustrate the feature interpretation process. Figure 5.b shows the canny edge and LBP extraction for given sample images. figure 5.c portrays the same features post feature selection, effectively mapped back for interpretation. This juxtaposition allows for a direct comparison, showcasing the impact of the feature selection process on the extracted features. It serves as a visual narrative of how the model prioritizes and refines features, shedding light on the interpretability of the chosen features.

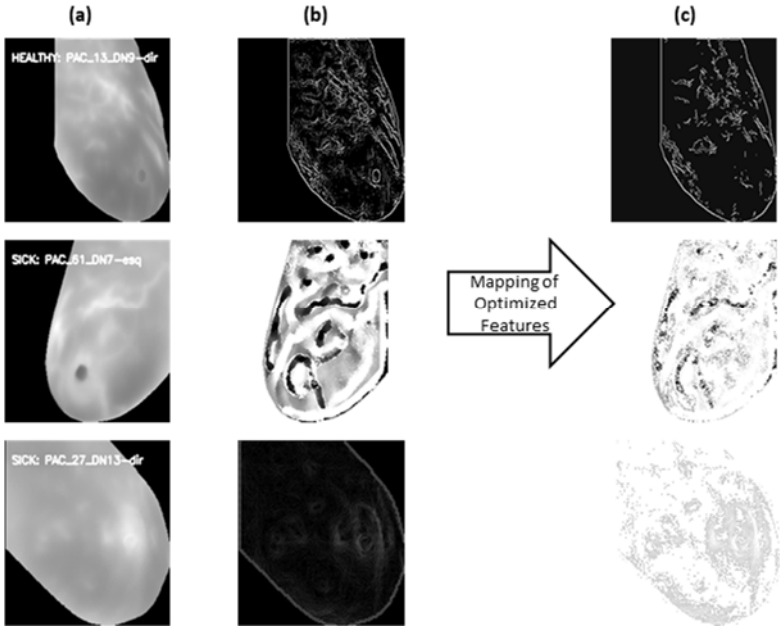

 doi:10.20944/preprints202408.2279.v1

Figure 5. (a) original cropped image ; (b) Feature Extract Image: Top using Canny Edges, Middle LBP extractor and Bottom using HOG; (c): Selected Features mapped back to Extracted Features.

Figure 6 and Figure 7 show the quantifiable aspects of feature in the image data. The upper part of Figure 6 presents a chart depicting the extracted features. Complementing this, the lower part of the figure exhibits the feature graph of the selected features after the metaheuristic-based optimization process. This clear differentiation between the extracted and selected features allows for a look into the model's preference for certain features over others. Within both figures, the blue bars represent features of the sample healthy image, while red bars are for a different sample image of sick category.

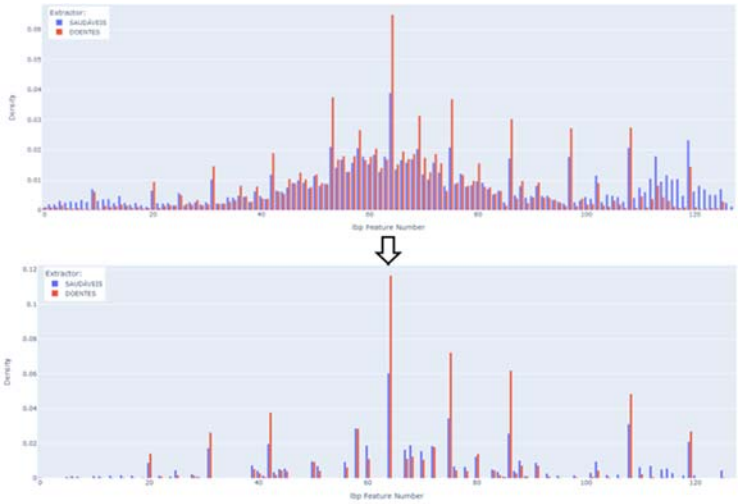

Figure 6. Example feature selection; Top: Extracted Features using LBP extractor; Bottom: Selected Features using HSMO.

The integration of SHAP values into the optimization process allows for a more informed selection of features based on the importance of individual features as determined for distinguishing between classes. Figure 7 is an example of a Feature Impact Visualization, using a SHAP dependency plot.

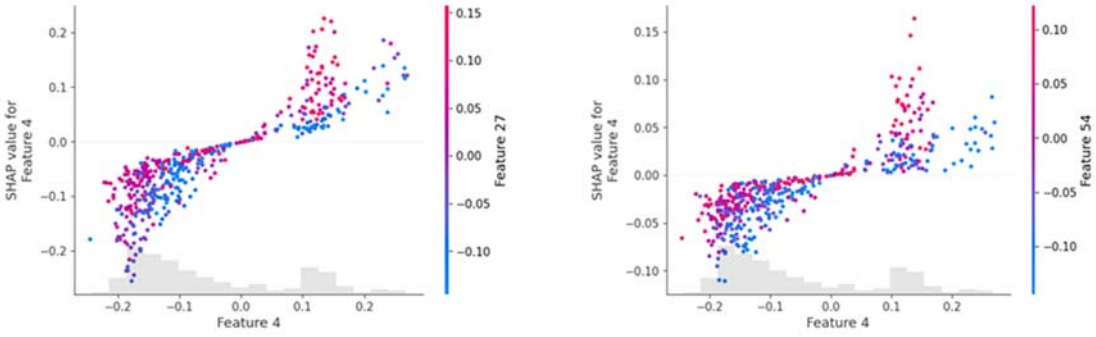

Figure 7. Example of explaining prediction using SHAP plot: The left side after applying HSMO optimization; the right side without optimization, both using a HOG feature extractor. The X-axis represents the value of Feature 4, and the Y-axis shows its SHAP value, indicating its contribution to the model's prediction. The color gradient represents secondary features (Feature 27 in the left plot and Feature 54 in the right plot), showing their interaction with Feature 4. The optimized model (left) displays a clearer and more structured relationship between features.

4. Experimental Setup

 doi:10.20944/preprints202408.2279.v1

The experimental setup consists of multiple parts each with respective configurations and settings. Data loading, dataset split approaches and feature extractors have previously been discussed in earlier sections. The extracted features are then fed into an optimization pipeline; which consists of feature selection, feature classification through machine learning using SVM polynomial kernel and objective function for optimization purpose .

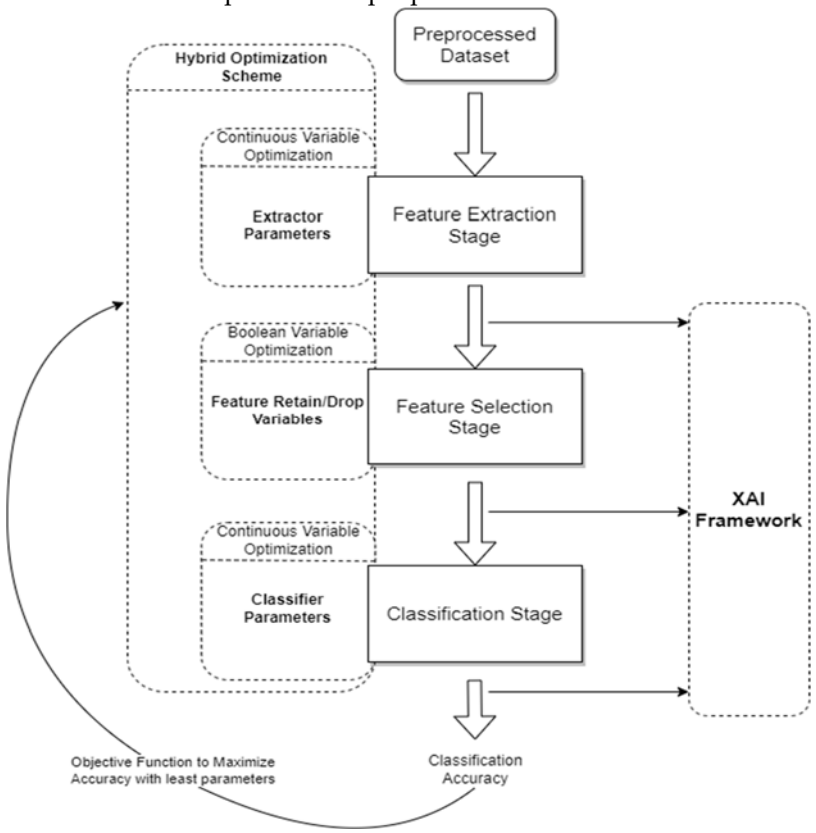

Figure 8. Optimization Process Flow

For each experiment, the optimization algorithms consist of the HSMO, HPSO, BPSO and BSMO. This section includes discussion and details of each of the remaining experiment components. The process illustrated in Figure 8 includes the remaining experimental setup block of the XAI framework. This framework takes parameters from each stage as indicated in order to provide the two-pronged interpretability functions. The classification stage XAI inputs correspond to utilization of SHAP to calculate feature importance, while the feature selection and extraction stage XAI inputs correspond to backwards mapped selection of features to make the decision more interpretable. The optimization flow pipeline indicates one iteration of the complete process. In effect, as metaheuristic algorithms are designed, the optimization process of both continuous and binary variables is carried out in multiple iterations so that the process improves iteratively (see Figure 9). Visualizing the process itself over each stage can be thought of as modifying values of all optimization variables over the iterations.

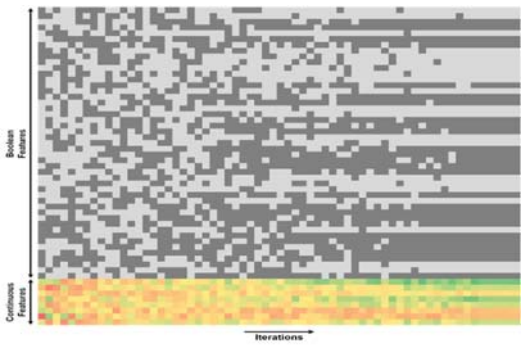

 doi:10.20944/preprints202408.2279.v1

Figure 9. Optimized Feature Selection and Hyperparameter process

The following Table 2 describes the parameters where boolean variables switch between True/False states and continuous variables get adjusted over their ranges.

Table 2. Details about method used in different stages with arguments and hyperparameters range.

CAD Steps	Methods	Feature Variables	Vaiables/ or constraints
Feature Extraction	LBP	Radius	8; [2,24]:2
		Points	60; [100,550]:10
	HOG	Orientations	9, [9,18]:1
		Pixels per cell	8, [2,16]:1
		Cells per block	4, [2,5]:1
	Gabor Filter	K-size: Size of the Gabor kernel. Larger values capture more spatial frequencies but also increase computational complexity	80; [20, 190] :20
		Sigma: Standard deviation of the Gaussian envelope. It controls the spread of the filter.	2.5, [0.10, 7]:0.10
		Theta: Orientation of the normal to the parallel stripes of a Gabor function. It determines the orientation of the features to be detected.	40, [0.1, 46]:2
		lamda: Wavelength of the sinusoidal factor. It affects the frequency of the feature to be detected	1.6; [0.2, 8]:0.5
		Gamma: Spatial aspect ratio. It controls the ellipticity of the filter	90, [8, 250]:0.5
	Canny Edge	Aperture size: the size of the Sobel kernel used for gradient computation	4; [7,80]:1
		Aperture transition: represents the transition range for adjusting the lower threshold during edge detection	2;[2,10]:2
		Aperture transition steps: This parameter specifies the number of steps or iterations used for adjusting the aperture transition range. It determines the granularity of the optimization process for the aperture transition	60;[10,120]:1
Feature Selection	The number of selected features by optimizer	128 Binary variables	True for included / False for not-included feature

 doi:10.20944/preprints202408.2279.v1

Classification	SVM	C: Regularization parameter. Controls the trade-off between training error and margin.	100; [10,7500]:10
		Coef0: Independent term in the kernel function	4; [1e-06, 4]:0.5
		Tolerance: determines the convergence criterion for the model training	1e-6; [1e-6, 4e-2]: 9e-4
		Degree: represents the degree of the polynomial function used in the kernel	3; [2, 10]:1

* The format of range is : Defalut Value; [min Value, max Value]: step size.

Following the extraction of features, they undergo a feature selection stage where each feature is treated as a boolean variable. Depending on whether the value is True or False, the corresponding feature is either retained or discarded. These boolean variables are collectively optimized by the optimization algorithms as well. The retained features are then used for training of classifiers and subsequent testing based on dataset splits. The resulting accuracy and other metrics such as F1 score, precision, recall are then fed into an objective function, that includes the number of selected parameters into computing a final resulting metric that is used by optimizers.

The objective function is designed to equally prioritize both high accuracy and a lower number of selected features through the use of the geometric mean, detailed as follows:

$$Fitness\ Score = 1 - \sqrt{Acc} \times \sqrt{FL} \quad (1)$$

$$FL = 1 - \frac{SF}{TF}$$

In this formulation, the fitness score represents the assessment of a specific solution set offered by the proposed optimization algorithm. The multi-objective function in Equation (1) denotes the geometric mean GM of two components: accuracy Acc and feature loss FL . FL quantifies the proportion of features that are not retained for the classification task. It is calculated by subtracting 1 from the ratio of the number of selected features SF to the total number of features TF. To align with the convention in optimization problems, where the objective is typically aimed towards zero, the fitness score is subtracted from 1. This approach yields a better potential solution in our optimization problem, achieving a desirable trade-off between accuracy and feature selection simultaneously.

5. Results and Discussion

The presentation of our research findings is structured into two distinct parts, both offering valuable insights into the performance and characteristics of the applied methodologies and conducted experiments. In the first segment, we explore the effectiveness of metaheuristic algorithms with a novel hybrid approach HSMO, HPSO coupled with the feature extraction methods. The aim was to evaluate the consistency of results across diverse optimization strategies. Multiple experiments were tested on the DMR-IR dataset. The positive class represents instances of sick breasts (red color). Therefore, to optimize the balance between computational resources and the desired level of performance, it was deemed sufficient to limit the optimization process to 60 iterations, as the incremental benefits beyond this point were deemed negligible. The experiment was conducted using Google Colab, powered by a Tesla4 GPU accelerator.

Figure 10 shows a chart indicating the resulting reduction in samples, as well as what the reduction translates to in terms of visual interpretation of the LBP, HOG, Gabor, and edge

 doi:10.20944/preprints202408.2279.v1

features. It can be seen that the histogram of feature importance distribution using HSMO and HPSO show similar shapes. in the case of HOG extractor , the feature counts ranging between 0 and 0.27. The highest peaks occur within bins 13 to 25 for both healthy and sick instances. For HSMO, the majority of counts fall within the lower end of this range, indicating that HSMO tends to favor a sparse selection of features by focusing on those that significantly contribute to the model's prediction. The HSMO optimizer demonstrates a more defined feature density distribution, due to its inherent properties to balance exploration and exploitation. On the other hand, HPSO demonstrates a more active exploration approach.The presence of higher counts beyond the primary peak range reflects HPSO’s tendency toward broader exploration, driven by its selection pressure mechanisms.

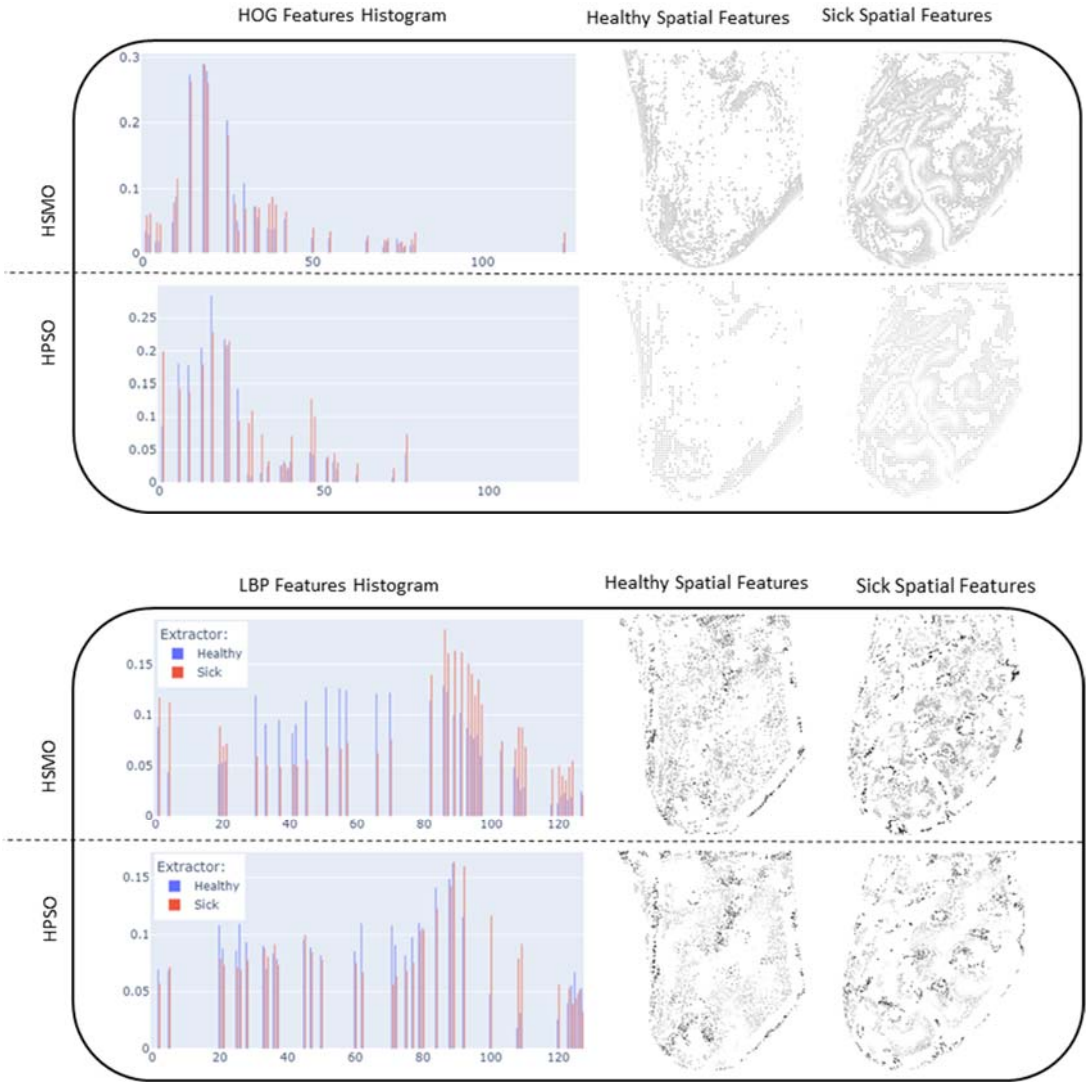

 doi:10.20944/preprints202408.2279.v1

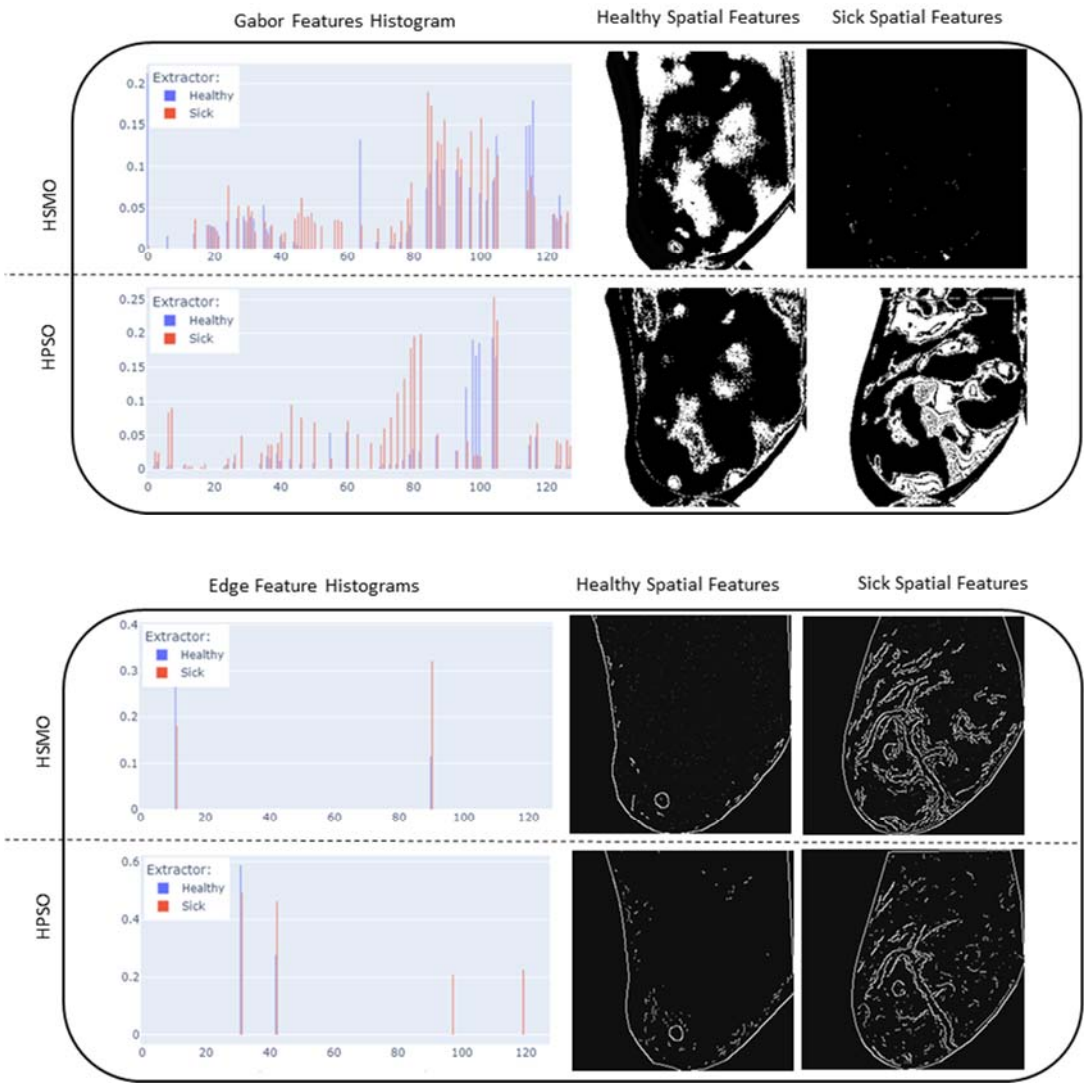

Figure 10. Resulting of Feature Histograms and Optimized Feature Mapping for LBP, HOG, Edge Extractors and Gabor.

The aggregated results across 60 optimizer runs for each extractor, as illustrate in Table 3, indicate that HSMO achieves leading performance in accuracy while maintaining a similar reduction in features compared to HPSO. Notably, the HSMO based HOG achieved a maximum geometric mean of 85.40%, an accuracy of 98.27% and F1- score of 98.15%, with only 25.78% of features. In comparison, HPSO achieved a slightly lower accuracy of 95.02% and F1-score of 94.71%.

Although HPSO provides a balanced outcome, but tends to a more aggressive feature reduction and still achieves competitive accuracy, for example, 95.89% for LBP with only 23.44% of features.

The lower accuracy observed with BPSO and BSMO compared to the proposed hybrid approach HPSO and HSMO stems from the fact that these methods are restricted to their fixed search space and limited dynamic capability, which results in suboptimal solutions, limited exploration and an inability to handle continuous variables effectively. For instance, the best accuracy ahieved for LBP-BSMO is 93.94% with a higher feature retention of 28.91%. This result underscores that binary optimization methods lacks the flexibility needed to adapt continuously and refine solutions effectively.

Table 3. Results of optimization process using diverse feature extraction methods.

Feature Extractor	Optimizer aproach	Hyperparameter tuning					Remaining Features (%)	Accuracy (%)	F1-Score (%)	Geometric Mean
		C	degree	Coef0	Tolerance	Feature parameter				
LBP	BSMO	Default parameter					28.91	93.94	93.33	0.8172022148770768
	BPSO	Default parameter					24.22	92.42	91.65	0.836874399178275
	HSMO	4050.0	4.0	3.0	0.012	Radius: 14.0 Point: 240.0	26.56	97.62	97.49	0.7169212799999999
	HPSO	3880.0	7.0	3.0	0.002	Radius: 14.0 Point: 330.0	**23.44**	95.89	95.67	0.73413384
Gabor Filters	BSMO	Default parameter					35.16	64.94	64.63	0.6488998073662836
	BPSO	Default parameter					32.81	63.64	0.63	0.6539091374189535
	HSMO	1820.0	6.0	1.4	0.0004	size: 180.0 sigma: 6.9 theta: 2.0 lamda: 8.0 gamma: 249.0	39.06	85.5	83.78	0.7218289271011518
	HPSO	7110.0	6.0	1.5	0.011	size: 40.0 sigma: 5.2 theta: 2.0 lamda: 4.5 gamma: 348.5	33.59	83.33	81.97	0.7439049199998613
HOG	BSMO	Default parameter					31.25	93.29	92.91	0.8008550118467137
	BPSO	Default parameter					32.81	91.34	90.99	0.7833986596873905
	HSMO	410.0	5.0	2.0	0.022	Orientations: 12.0 Pixels per cell: 2.0 Cells per block: 3.0	25.78	**98.27**	**98.15**	**0.8540257256078414**
	HPSO	730.0	13.0	1.5	0.033	Orientations: 14.0 Pixels per cell: 3.0 Cells per block: 5.0	25.78	95.02	94.71	0.8397847581374646
	BSMO	Default parameter					32.03	88.31	88.31	0.7747535543642249

doi:10.20944/preprints202408.2279.v1

Canny Edge	BPSO	Default parameter					39.06	89.39	89.28	0.7380668397916275
	HSMO	2380.0	6.0	1.5	0.009	Aperture size: 37.0 Aperture transition: 2.0 Aperture transition steps:10.0	37.5	91.99	91.04	0.7582463320056353
	HPSO	1770.0	4.0	4.5	0.006	Aperture size:16.0 Aperture transition: 4.0 Aperture transition steps: 12.0	32.03	85.71	83.33	0.7632633031922863

doi:10.20944/preprints202408.2279.v1

 doi:10.20944/preprints202408.2279.v1

Additionally, in order to include another layer of explainability at this stage, SHAP was used to analyze distribution of feature importance of selected features across the dataset. This step allowed to assess whether the use of metaheuristic algorithms had an impact on importance distribution of selected features. Figure 11 indicates the respective feature importance charts of LBP features using BSMO, BPSO, HSMO and HPSO optimizer .

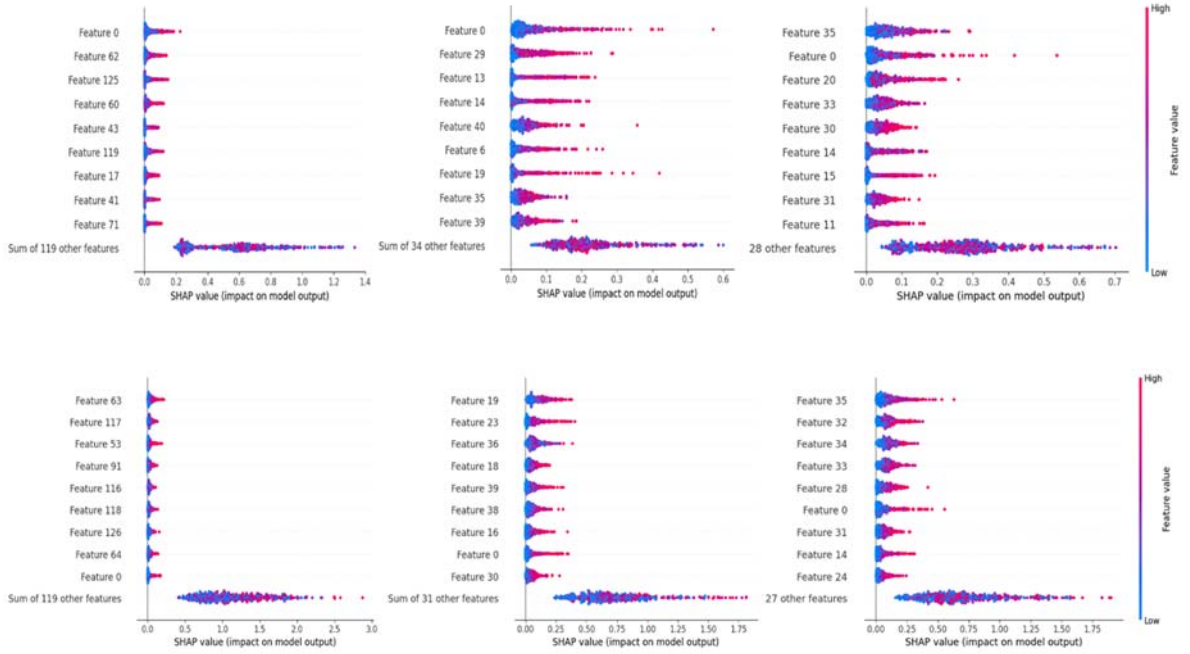

Figure 11. Top: without Optimization; left Full features; middle BSMO and right BPSO ; Bottom: with Optimization; left Full features; middle HSMO and right HPSO features.

A visible difference can be seen, where the distribution of remaining features in each metaheuristic algorithm tends to move towards greater importance scores. Most notable change occurs for HSMO and HPSO optimizes. These results also re-establish the fact that importance scores alone can't be used as a metric for feature selection, as evident from the above figure in which almost none of the most important deemed features of full feature set were selected during optimization by all the optimization algorithms. Though the distribution of importance scores still holds an effective role to assess how well the selection process performed for each algorithm comparatively.

Moving on to the second part of our results, we focused on the application of the leading optimization algorithm, HSMO, with various feature extractors. As the features still remain numerous even after being optimized, in order to gain this insight, SHAP was once again used to distinctly map the per instance ranked distribution of impact score from each top feature of each extractor as indicated in Figure 12 for Edge Filters, Gabor Filters, HOG, and LBP respectively. The feature importance illustrations are presented in the form of heatmaps, with their placement being controlled through SHAP in a logical way in order to highlight any arising patterns. The bars on the right of each heatmap indicate the individual impact of the listed feature in classification as a whole. Since the feature distribution becomes unique for each extractor, therefore in order to assess the impact of optimization, each of the heatmaps is shown in pairs where right heatmap indicates heatmap of all features and left indicates the heatmap of optimized features.

 doi:10.20944/preprints202408.2279.v1

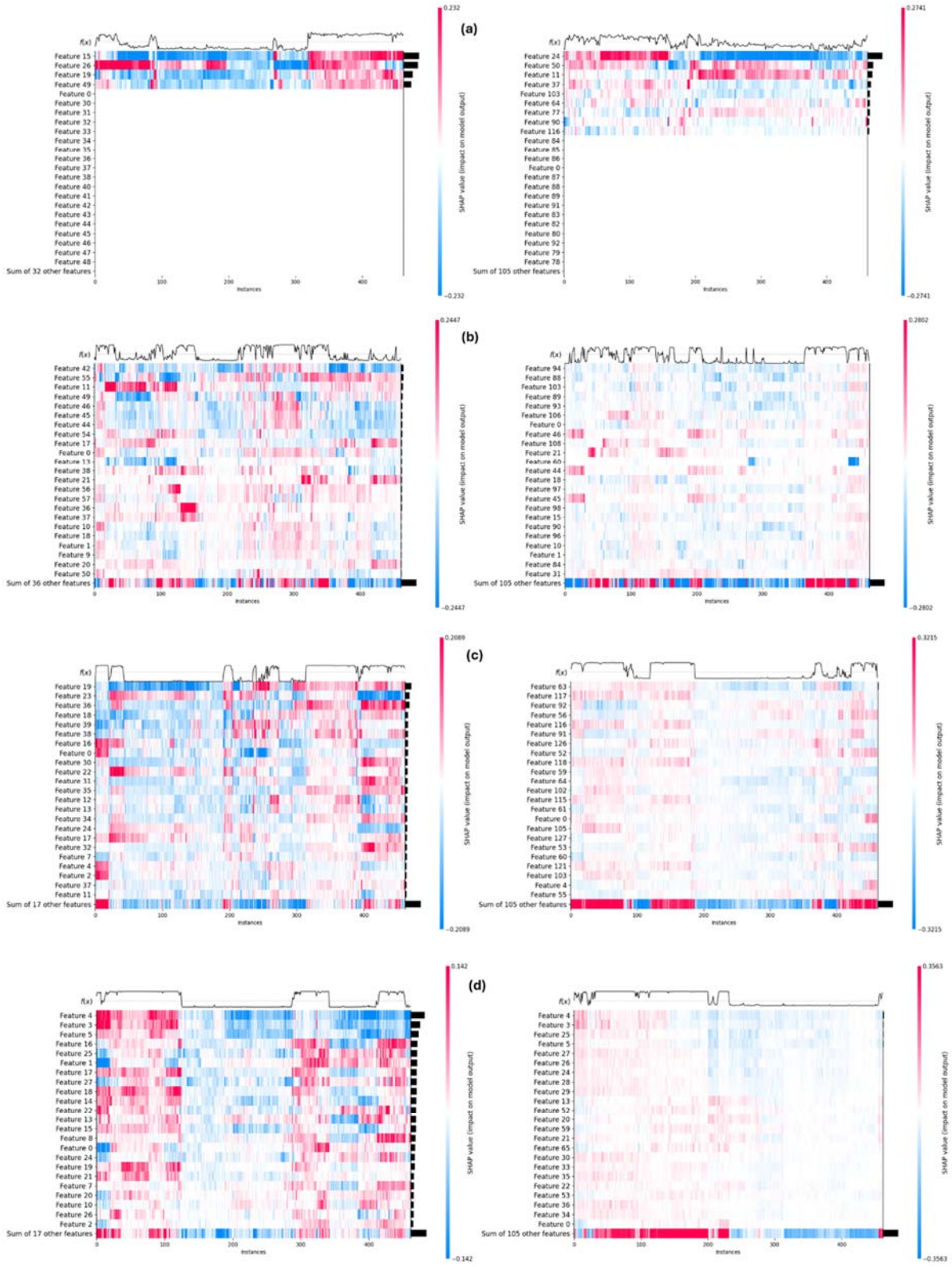

Figure 12. Feature Heatmap using HSMO optimizer: a) Canny Edge Detector, b) Gabor Filters, c) LBP; d) HOG – Full and Optimized Feature Heatmaps in Right and Left respectively.

As can be seen in Figure 12-a, the most distinctive features were extracted through edge detection. Optimization of these extracted features resulted in selection of key features, which can be seen from the top few optimized features being almost as important as all the low ranked features.

 doi:10.20944/preprints202408.2279.v1

Gabor Filters fared the worst out of these, perhaps due to limited search space (Figure 12-b), as their ability to gauge textures requires a much larger explorative search. Another reason can be that the extractor is being applied on thermal gradient rather than images themselves. The full feature set heatmap indicates the scattered impact across features with no specific descriptors arising. Optimization of these features improves the situation nonetheless by shedding features that might have been serving as noise to features that held valuable information and impact.

In Figures 12-c and 12-d, the HOG and LBP extractors enable the model to capture the most significant features, leading to clear and decisive predictions. The structure of their full feature heatmaps reflects this, particularly in the confidence function at the top of the heatmaps, which show a transitions from instances classified as healthy to those classified as sick in a much more defined way. The transition is especially sharp in the HOG heatmap, where the most distinctive features were extracted, which allowed for evident increase in accuracy. The optimization process further refined these features, selecting key ones that contribute significantly to the model's performance. This is evident as the top optimized features hold nearly as much importance as all the low-ranked features combined. As a result, the model's confidence transition becomes steeper as it crosses the boundary where instance change class, indicating a well-learned, generalizable pattern. This consistent and precise decision boundary is crucial in a CAD system, as it enhances the trust medical professionals place in the system's outputs, ultimately improving the system's reliability in clinical settings.

6. Conclusion

In conclusion, this research has resulted in insights into the synergy between metaheuristic algorithms and eXplainable Artificial Intelligence (XAI) for addressing multiobjective problems involving both continuous and boolean variables. The key findings and their implications underscore the importance of thoughtful algorithm selection, feature extraction, and interpretability, while maintaining transparency in use of metaheuristics.

The metaheuristic algorithm comparison revealed that the proposed Hybrid Particle Swarm Optimization (HPSO), and the proposed Hybrid Spider-Monkey Optimization (HSMO), HSMO consistently outperformed others in diverse problem scenarios. This superiority was further validated through XAI, particularly by employing SHAP to analyze feature importance distributions. Notably, optimizing through metaheuristics surpassed the direct use of SHAP-importance values, emphasizing the relationship between optimization and interpretability.

The impact of feature extractors (Local Binary Pattern, Histogram of Oriented Gradients, Edge Filters, Gabor Filters) was investigated, with Gabor Filters performing the least favorably, Edge Filters offering distinctive features, and LBP/HOG providing comprehensive sets of features. Corroborated by SHAP analysis, manifested through importance heatmaps, substantiating the significance of feature selection and extraction.

Furthermore, the study reinforces the contribution of feature extraction and optimization in tandem with metaheuristics, consistently improving model performance. These collective findings underscore the important ties between algorithmic choices, interpretability, and feature representation in addressing complex problems.

In terms of contributions to the field of Explainable AI, this research not only showcases the efficacy of HSMO but also emphasizes the integration of XAI methodologies, enhancing result interpretability, alongside of metaheuristics. These contributions extend beyond algorithmic performance alone, enriching the understanding of model decisions and facilitating broader adoption in practical applications.

For future work, this study can be expanded to multiple datasets beyond breast cancer detection to ensure the robustness of the proposed approach. Additionally, incorporating domain experts in the interpretability loop analysis can result invaluable insights to the decision making process of experts and learning acquired by ML models. Exploring additional extractors or their combinations, collectively optimized, also holds promise for further enhancing the proposed framework's efficacy.

In summary, this research not only advances understanding of the relationship between metaheuristic algorithms and XAI but also lays a foundation for continued exploration in the

collective domains Explainable AI, metaheuristics, and medical image analysis. The insights garnered contribute to the ongoing efforts to make computational models and metaheuristic algorithms more transparent, interpretable, and applicable in real-world contexts.

References

1. Ciatto S, Rosselli Del Turco M, Zappa M. The detectability of breast cancer by screening mammography. *Br J Cancer*. 1995;71(2):337-339. doi:10.1038/bjc.1995.67
2. Foxcroft LM, Evans EB, Joshua HK, Hirst C. BREAST CANCERS INVISIBLE ON MAMMOGRAPHY. *ANZ J Surg*. 2000;70(3):162-167. doi:10.1046/j.1440-1622.2000.01763.x
3. Pataky R, Phillips N, Peacock S, Coldman AJ. Cost-effectiveness of population-based mammography screening strategies by age range and frequency. *Journal of Cancer Policy*. 2014;2(4):97-102. doi:10.1016/j.jcpo.2014.09.001
4. Pauwels EKJ, Foray N, Bourguignon MH. Breast Cancer Induced by X-Ray Mammography Screening? A Review Based on Recent Understanding of Low-Dose Radiobiology. *Med Princ Pract*. 2015;25(2):101-109. doi:10.1159/000442442
5. Dabbous FM, Dolecek TA, Berbaum ML, et al. Impact of a False-Positive Screening Mammogram on Subsequent Screening Behavior and Stage at Breast Cancer Diagnosis. *Cancer Epidemiol Biomarkers Prev*. 2017;26(3):397-403. doi:10.1158/1055-9965.EPI-16-0524
6. Bansal R, Collison S, Krishnan L, et al. A prospective evaluation of breast thermography enhanced by a novel machine learning technique for screening breast abnormalities in a general population of women presenting to a secondary care hospital. *Frontiers in Artificial Intelligence*. 2023;5. Accessed February 25, 2023. https://www.frontiersin.org/articles/10.3389/frai.2022.1050803
7. Da Luz TGR, Coninck JC, Ulbricht L. Comparison of the Sensitivity and Specificity Between Mammography and Thermography in Breast Cancer Detection. In: Bastos-Filho TF, de Oliveira Caldeira EM, Frizera-Neto A, eds. *XXVII Brazilian Congress on Biomedical Engineering*. IFMBE Proceedings. Springer International Publishing; 2022:2163-2168. doi:10.1007/978-3-030-70601-2_316
8. Arora N, Martins D, Ruggerio D, et al. Effectiveness of a noninvasive digital infrared thermal imaging system in the detection of breast cancer. *Am J Surg*. 2008;196(4):523-526. doi:10.1016/j.amjsurg.2008.06.015
9. Head JF, Elliott RL. Infrared imaging: making progress in fulfilling its medical promise. *IEEE Engineering in Medicine and Biology Magazine*. 2002;21(6):80-85. doi:10.1109/MEMB.2002.1175142
10. Sarigoz T, Ertan T, Topuz Ö, Sevim Y, Cihan Y. Role of Digital Infrared Thermal Imaging in the Diagnosis of Breast Mass: A Pilot Study. *Infrared Physics & Technology*. 2018;91. doi:10.1016/j.infrared.2018.04.019
11. Guetari R, Ayari H, Sakly H. Computer-aided diagnosis systems: a comparative study of classical machine learning versus deep learning-based approaches. *Knowl Inf Syst*. 2023;65(10):3881-3921. doi:10.1007/s10115-023-01894-7
12. Retson TA, Eghtedari M. Expanding Horizons: The Realities of CAD, the Promise of Artificial Intelligence, and Machine Learning's Role in Breast Imaging beyond Screening Mammography. *Diagnostics*. 2023;13(13):2133. doi:10.3390/diagnostics13132133
13. Skjong R, Wentworth BH. Expert Judgment And Risk Perception. In: OnePetro; 2001. Accessed November 11, 2023. https://dx.doi.org/
14. Park H, Megahed A, Yin P, Ong Y, Mahajan P, Guo P. Incorporating Experts' Judgment into Machine Learning Models. *Expert Systems with Applications*. 2023;228:120118. doi:10.1016/j.eswa.2023.120118
15. Barredo Arrieta A, Díaz-Rodríguez N, Del Ser J, et al. Explainable Artificial Intelligence (XAI): Concepts, taxonomies, opportunities and challenges toward responsible AI. *Information Fusion*. 2020;58:82-115. doi:10.1016/j.inffus.2019.12.012
16. Yang G, Ye Q, Xia J. Unbox the black-box for the medical explainable AI via multi-modal and multi-centre data fusion: A mini-review, two showcases and beyond. *Information Fusion*. 2022;77:29-52. doi:10.1016/j.inffus.2021.07.016
17. Koh DM, Papanikolaou N, Bick U, et al. Artificial intelligence and machine learning in cancer imaging. *Commun Med*. 2022;2(1):1-14. doi:10.1038/s43856-022-00199-0
18. Tsai CW, Chiang MC, Ksentini A, Chen M. Metaheuristic Algorithms for Healthcare: Open Issues and Challenges. *Computers & Electrical Engineering*. 2016;53:421-434. doi:10.1016/j.compeleceng.2016.03.005
19. Dihmani H, Bousselham A, Bouattane O. A Review of Feature Selection and HyperparameterOptimization Techniques for Breast Cancer Detection on thermograms Images. In: *2023 IEEE 6th International Conference on Cloud Computing and Artificial Intelligence: Technologies and Applications (CloudTech)*. ; 2023:01-08. doi:10.1109/CloudTech58737.2023.10366143
20. Ezenkwu CP, Akpan UI, Stephen BUA. A class-specific metaheuristic technique for explainable relevant feature selection. *Machine Learning with Applications*. 2021;6:100142. doi:10.1016/j.mlwa.2021.100142
21. Aranha C, Camacho Villalón CL, Campelo F, et al. Metaphor-based metaheuristics, a call for action: the elephant in the room. *Swarm Intell*. 2022;16(1):1-6. doi:10.1007/s11721-021-00202-9

22. Del Ser J, Osaba E, Molina D, et al. Bio-inspired computation: Where we stand and what's next. *Swarm and Evolutionary Computation*. 2019;48:220-250. doi:10.1016/j.swevo.2019.04.008
23. Deb K. Multi-Objective Optimization Using Evolutionary Algorithms: An Introduction.
24. London AJ. Artificial Intelligence and Black-Box Medical Decisions: *Accuracy versus Explainability*. *Hastings Center Report*. 2019;49(1):15-21. doi:10.1002/hast.973
25. Kallianos K, Mongan J, Antani S, et al. How far have we come? Artificial intelligence for chest radiograph interpretation. *Clinical Radiology*. 2019;74(5):338-345. doi:10.1016/j.crad.2018.12.015
26. Zucco C, Liang H, Fatta GD, Cannataro M. Explainable Sentiment Analysis with Applications in Medicine. In: *2018 IEEE International Conference on Bioinformatics and Biomedicine (BIBM)*. ; 2018:1740-1747. doi:10.1109/BIBM.2018.8621359
27. Hu S, Gao Y, Niu Z, et al. Weakly Supervised Deep Learning for COVID-19 Infection Detection and Classification From CT Images. *IEEE Access*. 2020;8:118869-118883. doi:10.1109/ACCESS.2020.3005510
28. Langlotz CP, Allen B, Erickson BJ, et al. A Roadmap for Foundational Research on Artificial Intelligence in Medical Imaging: From the 2018 NIH/RSNA/ACR/The Academy Workshop. *Radiology*. 2019;291(3):781-791. doi:10.1148/radiol.2019190613
29. Ali S, Abuhmed T, El-Sappagh S, et al. Explainable Artificial Intelligence (XAI): What we know and what is left to attain Trustworthy Artificial Intelligence. *Information Fusion*. 2023;99:101805. doi:10.1016/j.inffus.2023.101805
30. Hasan MdK, Ahamad MdA, Yap CH, Yang G. A survey, review, and future trends of skin lesion segmentation and classification. *Computers in Biology and Medicine*. 2023;155:106624. doi:10.1016/j.compbiomed.2023.106624
31. Brunese L, Mercaldo F, Reginelli A, Santone A. Explainable Deep Learning for Pulmonary Disease and Coronavirus COVID-19 Detection from X-rays. *Computer Methods and Programs in Biomedicine*. 2020;196:105608. doi:10.1016/j.cmpb.2020.105608
32. Koyyada SP, Singh TP. An explainable artificial intelligence model for identifying local indicators and detecting lung disease from chest X-ray images. *Healthcare Analytics*. 2023;4:100206. doi:10.1016/j.health.2023.100206
33. Barata C, Celebi ME, Marques JS. Explainable skin lesion diagnosis using taxonomies. *Pattern Recognition*. 2021;110:107413. doi:10.1016/j.patcog.2020.107413
34. Nigar N, Umar M, Shahzad MK, Islam S, Abalo D. A Deep Learning Approach Based on Explainable Artificial Intelligence for Skin Lesion Classification. *IEEE Access*. 2022;10:113715-113725. doi:10.1109/ACCESS.2022.3217217
35. Abdel-Nasser M, Moreno A, Puig D. Breast Cancer Detection in Thermal Infrared Images Using Representation Learning and Texture Analysis Methods. *Electronics*. 2019;8(1):100. doi:10.3390/electronics8010100
36. Aidossov N, Mashekova A, Zhao Y, Zarikas V, Ng E, Mukhmetov O. Intelligent Diagnosis of Breast Cancer with Thermograms using Convolutional Neural Networks: In: *Proceedings of the 14th International Conference on Agents and Artificial Intelligence*. SCITEPRESS - Science and Technology Publications; 2022:598-604. doi:10.5220/0010920700003116
37. Kiymet S, Aslankaya MY, Taskiran M, Bolat B. Breast Cancer Detection From Thermography Based on Deep Neural Networks. In: *2019 Innovations in Intelligent Systems and Applications Conference (ASYU)*. IEEE; 2019:1-5. doi:10.1109/ASYU48272.2019.8946367
38. Aidossov N, Zarikas V, Zhao Y, et al. An Integrated Intelligent System for Breast Cancer Detection at Early Stages Using IR Images and Machine Learning Methods with Explainability. *SN COMPUT SCI*. 2023;4(2):184. doi:10.1007/s42979-022-01536-9
39. Aidossov N, Zarikas V, Mashekova A, et al. Evaluation of Integrated CNN, Transfer Learning, and BN with Thermography for Breast Cancer Detection. *Applied Sciences*. 2023;13(1):600. doi:10.3390/app13010600
40. Nicandro CR, Efrén MM, María Yaneli AA, et al. Evaluation of the Diagnostic Power of Thermography in Breast Cancer Using Bayesian Network Classifiers. *Computational and Mathematical Methods in Medicine*. 2013;2013:1-10. doi:10.1155/2013/264246
41. Dey S, Roychoudhury R, Malakar S, Sarkar R. Screening of breast cancer from thermogram images by edge detection aided deep transfer learning model. *Multimed Tools Appl*. Published online January 8, 2022. doi:10.1007/s11042-021-11477-9
42. Gonçalves CB, Souza JR, Fernandes H. CNN architecture optimization using bio-inspired algorithms for breast cancer detection in infrared images. *Computers in Biology and Medicine*. 2022;142:105205. doi:10.1016/j.compbiomed.2021.105205
43. Pramanik R, Pramanik P, Sarkar R. Breast cancer detection in thermograms using a hybrid of GA and GWO based deep feature selection method. *Expert Systems with Applications*. 2023;219:119643. doi:10.1016/j.eswa.2023.119643
44. Silva L, Saade D, Sequeiros Olivera G, et al. A New Database for Breast Research with Infrared Image. *Journal of Medical Imaging and Health Informatics*. 2014;4:92-100. doi:10.1166/jmihi.2014.1226

45. Zuluaga-Gomez J, Masry ZA, Benaggoune K, Meraghni S, Zerhouni N. A CNN-based methodology for breast cancer diagnosis using thermal images. *Computer Methods in Biomechanics and Biomedical Engineering: Imaging & Visualization,*. Published online 2020:16.
46. Dalal N, Triggs B. Histograms of oriented gradients for human detection. In: *2005 IEEE Computer Society Conference on Computer Vision and Pattern Recognition (CVPR'05)*. Vol 1. ; 2005:886-893 vol. 1. doi:10.1109/CVPR.2005.177
47. Ojala T, Pietikäinen M, Harwood D. A comparative study of texture measures with classification based on featured distributions. *Pattern Recognition*. 1996;29(1):51-59. doi:10.1016/0031-3203(95)00067-4
48. Daugman JG. Uncertainty relation for resolution in space, spatial frequency, and orientation optimized by two-dimensional visual cortical filters. *J Opt Soc Am A, JOSAA*. 1985;2(7):1160-1169. doi:10.1364/JOSAA.2.001160
49. Canny J. A Computational Approach to Edge Detection. *IEEE Transactions on Pattern Analysis and Machine Intelligence*. 1986;PAMI-8(6):679-698. doi:10.1109/TPAMI.1986.4767851
50. Bansal JC, Sharma H, Jadon SS, Clerc M. Spider Monkey Optimization algorithm for numerical optimization. *Memetic Comp*. 2014;6(1):31-47. doi:10.1007/s12293-013-0128-0
51. Kennedy J, Eberhart R. Particle swarm optimization. In: *Proceedings of ICNN'95 - International Conference on Neural Networks*. Vol 4. ; 1995:1942-1948 vol.4. doi:10.1109/ICNN.1995.488968
52. Singh U, Salgotra R, Rattan M. A Novel Binary Spider Monkey Optimization Algorithm for Thinning of Concentric Circular Antenna Arrays. *IETE Journal of Research*. 2016;62(6):736-744. doi:10.1080/03772063.2015.1135086
53. Kennedy J, Eberhart RC. A discrete binary version of the particle swarm algorithm. In: *Computational Cybernetics and Simulation 1997 IEEE International Conference on Systems, Man, and Cybernetics*. Vol 5. ; 1997:4104-4108 vol.5. doi:10.1109/ICSMC.1997.637339